Computation at a Coordinate Singularity

**Workshop on Numerical and Computational Methods for Simulation of All-Scale Geophysical Flows
ECMWF, Reading, October 3-6, 2016**

**JM Prusa: Teraflux Corporation
Boca Raton, FL
prusajm@gmail.com**

Motivation

Geodesic Grid, "spring" grid divergence error, (Tomita et.al, JCP 2001) + Lambert conformal mapping (Iga and Tomita, JCP 2014)
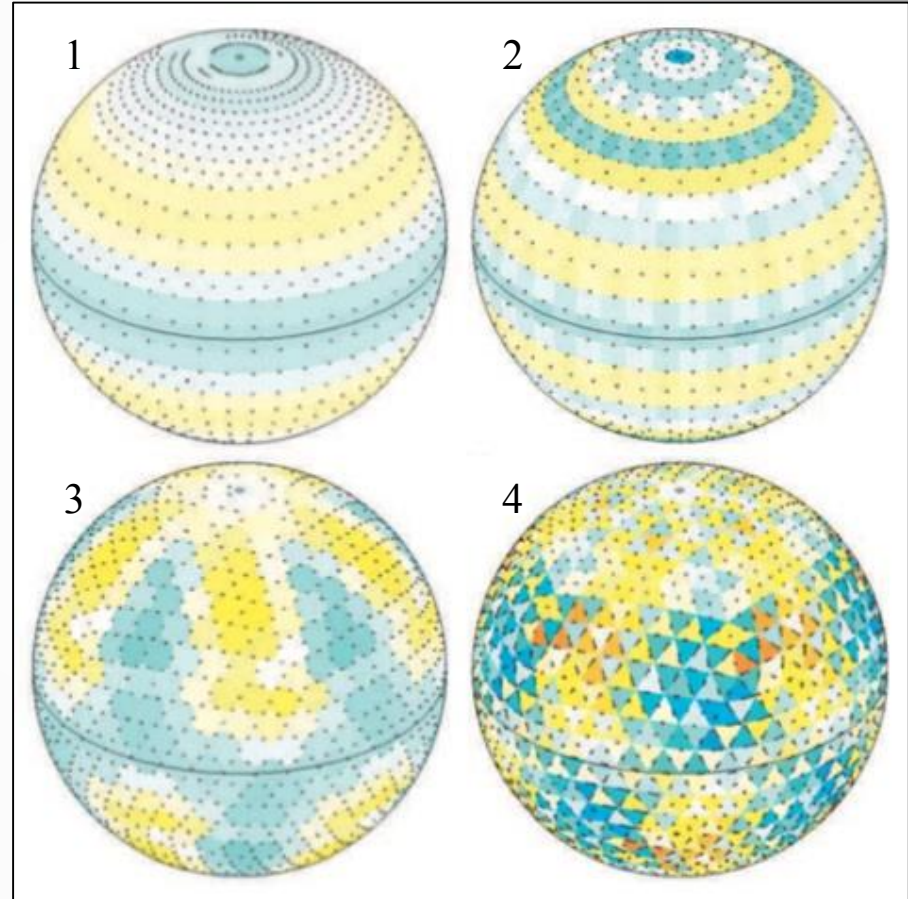
RIGHT: Figure shows relative height errors for nonlinear SWE's: 1. lat-lon grid. 2. lat-lon with "skipped" nodes at high latitudes. 3. hexagonal icosahedron. 4. triangular icosahedron (geodesic). Study used unstructured C-grid model TRiSK. (Weller et.al, JCP 2012.)

Presentation Outline

1. Background theory, *inner*, *middle*, and *outer* solutions for polar singularity of classical spherical polar parameterization of the sphere.

2. Computational model and Held-Suarez test case

3. Computational Results (STATS)

4. Summary

Theoretical Preliminaries: Continuity

$$\frac{1}{r\cos\phi}\frac{\partial u}{\partial\lambda} + \frac{1}{r\cos\phi}\frac{\partial(v\cos\phi)}{\partial\phi} + \frac{1}{r^2}\frac{\partial(r^2w)}{\partial r} = 0$$

transient term & compressibility not important here

expand 2nd term & rearrange:

$$\left(\frac{1}{r\cos\phi}\right)\left(\frac{\partial u}{\partial\lambda} - v\sin\phi\right) + \left(\frac{1}{r}\right)\left(\frac{\partial v}{\partial\phi} + \frac{1}{r}\frac{\partial(r^2w)}{\partial r}\right) = 0 \quad \text{(A)}$$

define $E = \varepsilon/R << 1$ and expand (sin, cos) in NP neighborhood $\pi/2 - E \; \delta \; \phi \; \delta \; \pi/2$

$$\sin\phi = 1 - E^2/2! + \dots$$
$$\cos\phi = E - \dots \quad \text{(B)}$$

substituting (B) into (A), and take lim E ⟶ 0⁺

$$\lim_{E\to0^+}\left(\frac{\partial u}{\partial\lambda} - v\right) = -\lim_{E\to0^+} E\left(\frac{\partial v}{\partial\phi} + \frac{1}{r}\frac{\partial(r^2w)}{\partial r}\right) = 0 \quad \rightarrow \quad \boxed{\frac{\partial u^+}{\partial\lambda} - v^+ = 0}$$

NOTE: (ϕ, λ) are meridonal , zonal coordinates

Theoretical Preliminaries: Vorticity (vertical component)

$$\omega_r = \frac{1}{r^2 \cos\phi}\left(\frac{\partial(rv)}{\partial\lambda} - \frac{1}{r}\frac{\partial(ru\cos\phi)}{\partial\phi}\right)$$

well defined even at the poles (consider a Cartesian description on the tangent plane B_ε)

expand 2nd term & rearrange:

$$r^2\omega_r = -\frac{\partial u}{\partial\phi} + \frac{1}{\cos\phi}\left(\frac{\partial(rv)}{\partial\lambda} + u\sin\phi\right) \quad \text{(A)}$$

define $E = \varepsilon/R << 1$ and expand (sin, cos) in NP neighborhood $\pi/2 - E \,\delta\, \phi \,\delta\, \pi/2$

$$\sin\phi = 1 - E^2/2! + \cdots$$
$$\cos\phi = E - \ldots \quad \text{(B)}$$

substituting (B) into (A), then take limit $E \longrightarrow 0^+$

$$\lim_{E\to 0^+}(r^2\omega_r) = -\lim_{E\to 0^+} E\left(\frac{\partial u}{\partial\phi}\right) + \lim_{E\to 0^+} E^{-1}\left(\frac{\partial v}{\partial\lambda} + u\right) \longrightarrow \boxed{\frac{\partial v^+}{\partial\lambda} + u^+ = 0}$$

Theoretical Preliminaries: INNER SOLUTION (u^+, v^+)

$$\frac{\partial u^+}{\partial \lambda} - v^+ = 0 \quad , \quad \frac{\partial v^+}{\partial \lambda} + u^+ = 0$$

immediately leads to "directional" *inner solution* for horizontal winds:

$$\boxed{u^+ = A\cos\lambda + B\sin\lambda \quad \text{and} \quad v^+ = B\cos\lambda - A\sin\lambda} \quad (A)$$

Note $\mathbf{V}_h^+ = u^+ \mathbf{e}_\lambda + v^+ \mathbf{e}_\phi$ has constant direction & magnitude $\forall \lambda$ in $[0, 2\pi)$

and zonally averaged STATS:

$$< u^+ > = 0 = < v^+ > \quad \text{and} \quad < (u^+)^2 > = (A^2 + B^2)/2 = < (v^+)^2 > \quad (B)$$

The vertical component of wind, w^+, behaves as a scalar and takes on a single value at the pole. All other scalars behave similarly.

All vectors (e.g., ***gradient***) behave as the wind field. For these geometrical objects, the singularity is a ***ring***.

The *middle solution* bridges the gap between the inner solution and the *outer solution* that is the full numerical result.
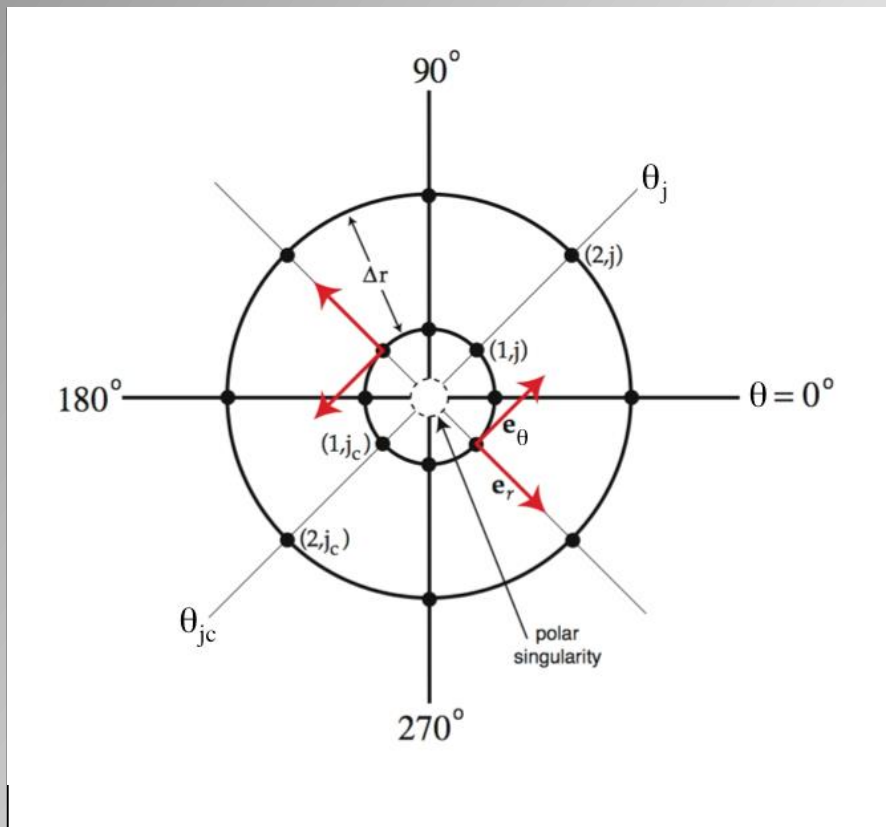
- prescribed spectral series for the dependent fields on the tangent disk B_ε, using a polar cylindrical parameterization (r, θ, z), $0 \le r \le \varepsilon$

- $\delta K = (\varepsilon K)^2/2 - (\varepsilon K)^4/24 + ...$ ($\delta = \Delta z$ error tangent disk to spherical cap; K = curvature)

- inner solution: exact boundary conditions at the pole

- numerical solution: generates spectral coefficients

Theoretical Preliminaries: MIDDLE SOLUTION

zonal wind to O(ε):
$$u_\varepsilon = u^+ + \alpha_1 r + (a_{12}\cos 2\theta + b_{12}\sin 2\theta)r$$

meridional wind to O(ε^3):
$$v_\varepsilon = v^+ + \beta_1 r + (b_{12}\cos 2\theta - a_{12}\sin 2\theta)r + (c_{21}\cos\theta + d_{21}\sin\theta)r^2$$
$$+ (b_{23}\cos 3\theta - a_{23}\sin 3\theta)r^2 + \beta_3 r^3 + (c_{32}\cos 2\theta + d_{32}\sin 2\theta)r^3$$
$$+ (b_{34}\cos 4\theta - a_{34}\sin 4\theta)r^3$$

NOTE PARITY: n+m = odd (for $r^n\cos (m\theta)$, ...); Boyd 2000

horizontal wind divergence to O(ε):
$$(\nabla \bullet V)_{h,\varepsilon} = 2\alpha_1 + [(3a_{21} + d_{21})\cos\theta + (3b_{21} - c_{21})\sin\theta]r$$

$$(\nabla \bullet V)_h^+$$

vertical vorticity to O(ε^2):
$$\omega_\varepsilon^3 = 2\beta_1 + [(-b_{21} + 3c_{21})\cos\theta + (a_{21} + 3d_{21})\sin\theta]r + 4\beta_3 r^2$$
$$+ 2[(-b_{32} + 2c_{32})\cos 2\theta + (a_{32} + 2d_{32})\sin 2\theta]r^2$$

$$\omega^+$$

NOTE PARITY: n+m = even (for $r^n\cos (m\theta)$, ...)

Preliminaries: OUTER SOLUTION MATCHING

transform horizontal coordinates: $(\theta \rightarrow \pm\lambda ; \pi/2 - r/R \rightarrow \pm\phi)$ NP+ SP-

➔ **for any dependent field the form:**

$$\varsigma_\varepsilon = A_0 + (A_1 \cos\lambda + B_1 \sin\lambda) + (A_2 \cos 2\lambda + B_2 \sin 2\lambda)$$
$$+ (A_3 \cos 3\lambda + B_3 \sin 3\lambda) + ...$$

Coefficients A_0, A_1, ... , B_0, ... are now $A_0(t, \phi, z)$, ... and are determined by fitting the corresponding spectral series to the full numerical solution.

PARITY RESTRICTIONS ON FORM!

2a. EULAG Model Features

- **Nonhydrostatic options**:
 (i) Lipps-Hemler (JAS 1982) anelastic equations
 (ii) fully compressible equations (Smolarkiewicz et al. JCP 2014); 3 "flavors" (explicit, semi-implicit, fully implicit)
(iii) pseudo-compressible(Durran JAS 1989)

- **Non-oscillatory forward-in-time advection**:
(i) Semi-Langrangian (SL) or
(ii) fully conservative Eulerian (MPDATA)helps to preserve monotonicity and eliminates nonlinear instability, default 2nd order in space and time.

- **turbulence closure options**: Direct Numerical Simulation (DNS), LES, or Implicit Large Eddy Simulation (ILES). ILES produces dissipation nonlinearly – just enough locally to avoid oscillations (uses limiters based upon the convexity of the flow).

- **Implicit treatment of gravity waves** via implicit integration of potential temperature perturbation

- **Grid adaptivity** via continuous remapping of coordinates

- **Preconditioned Krylov solver** (conjugate residual) for elliptic pressure perturbation equation → semi-implicit solver for p', $\mathbf{V}$, θ (dry anelastic simulation).

The new polar boundary conditions are tested in the implicit absorber in the pressure solver for the variables u, v, w, and θ.   This suggests a polar BC nomenclature for spectral modes: "abcd" for fields " $uvw\theta$".

examples: 3333 → zonal modes 0,1,2,3 used for all four variables
2⁻2⁻22 → zonal modes 1,2 used for (u, v) and 0,1,2 for (w, θ).
1⁻1⁻00 → zonal modes 1 used for (u, v) and 0 for (w, θ).

2b. Held-Suarez test case

(Held and Suarez, *BAMS* 1994)

- idealized dry climate for testing the dynamic cores of climate models
- prescribed idealized environmental profiles
- Rayleigh damping of low level winds (with a time scale of 1 day)
- Newtonian relaxation (with time scales of 4 and 40 days) of the temperature
- prescribed relaxations replace surface exchanges, as well as radiative and moist physics.

In spite of this simplicity, the climate develops into an approximately stationary, quasi-geostrophic state that replicates many of the essential features of the Earth's climate, such as the mean meridional circulation, equatorial easterlies, the zonal jets, fronts, barotropic blocking events, and gravity wave radiation from baroclinic instabilities.

3. Computational Results

Geostrophic Adjustment
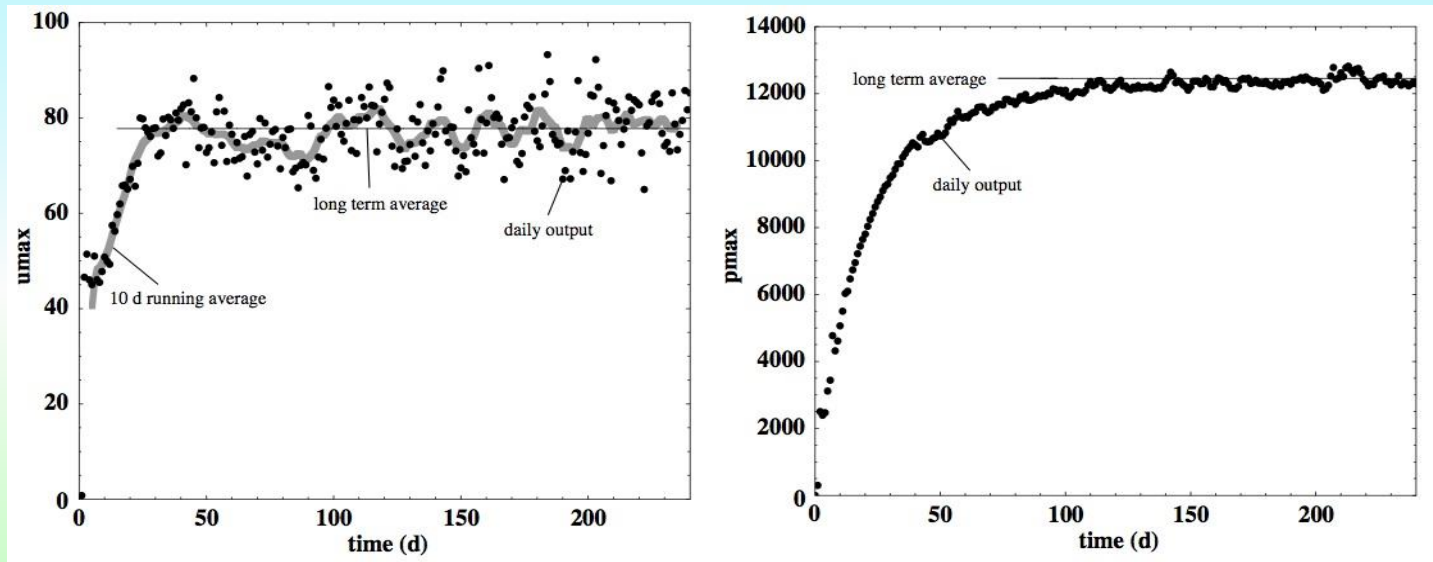
Spin-up of HS simulation. Left panel: u_{mx} in ms^{-1}, the 78 ms^{-1} long term average from 40 to 240 days contrasts with a 10 day running average that shows multi-day oscillations at periods ranging from 4 to 40 days. Right panel: p_{mx} refers to the maximum anelastic pressure perturbation, which approaches quasi-stationary statistics much later near day 150. Vertical wind development (not shown) is intermediate in its geostrophic adjustment qualities. (128 x 72) horizontal grid; 30 km depth with 41 vertical levels and exp. stretch ST first $\Delta z = 300$ m.

Maximum Courant number STATISTICS
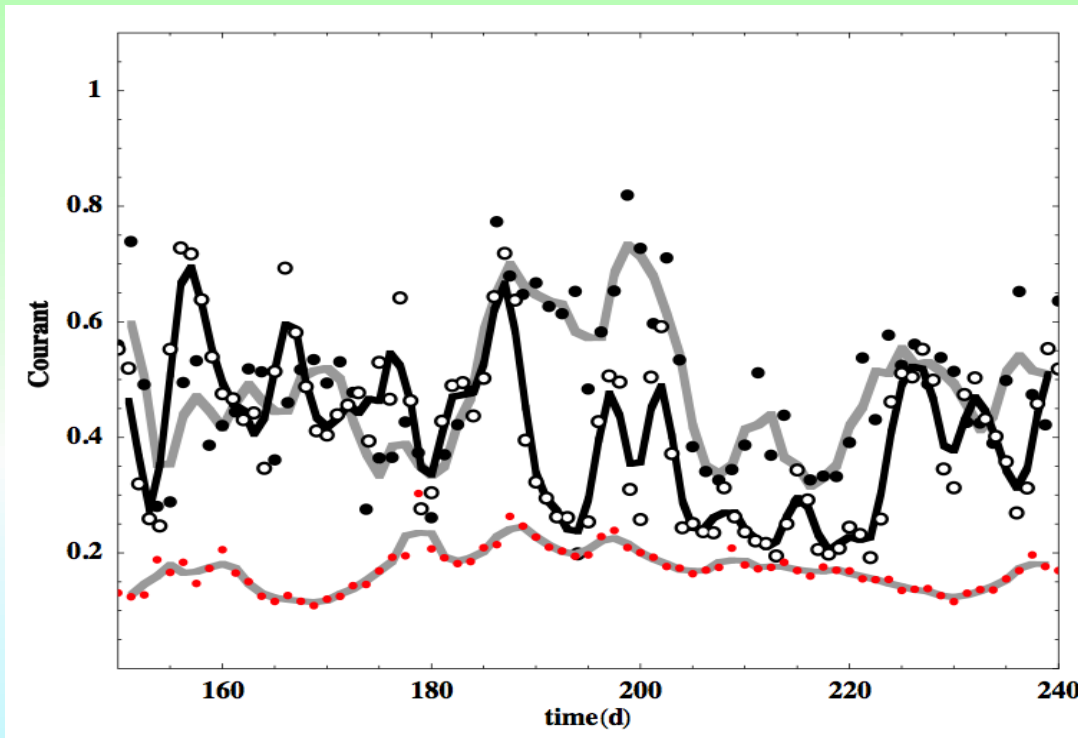
	control	pwave 2-2-22	zonave 0000
MX	0.82	0.72	0.30
AVE	0.49	0.39	0.17
MN	0.26	0.19	0.11
SD	0.13	0.13	0.04
SK	0.34	0.23	0.59

Comparison of CFL_{mx} based upon reference $\Delta t = 240s$ from three HS simulations: control (no absorber), 2−2−22 and 0000 (zonal averages only) implicit absorbers. The control run required $\Delta t = 180s$ to avoid CFL instability in this time interval and its CFL_{mx} has been multiplied by 1.333 in order to resale the results to the reference time step.

Surface Wind Data for Amundsen-Scott South Pole Station

Fig. 10. Daily mean resultant (vector) wind speed for 50-year climatology (1957–2006).
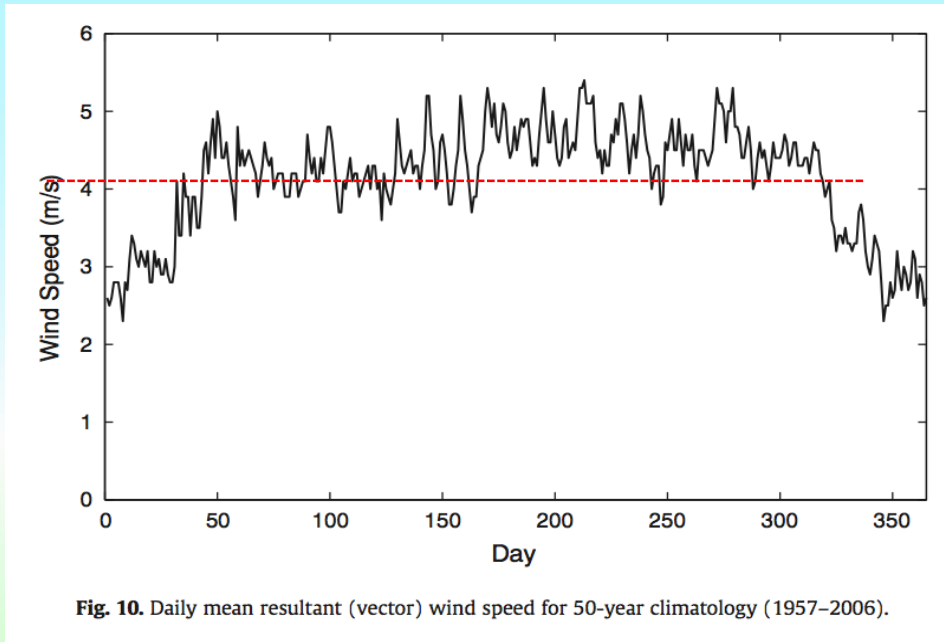
Daily Wind Statistics
(Lazzara et.al, *Atm. Res.* 2012)

February 1957-January 2011

NOTE: Publication corrected original meteorological records that contained time stamp errors; also improved daily temperature averaging.

Wind speed in ms⁻¹ (Uncorrected data 1958-2002 in parenthesis)

WIND TYPE	MIN	AVE	MAX
Daily MIN	(0.1)	(1.5)	(3.7)
Daily AVE	(1.5)	4.1	(11.1)
Monthly MAX	8.5		22.5

Model Surface Winds at North Pole
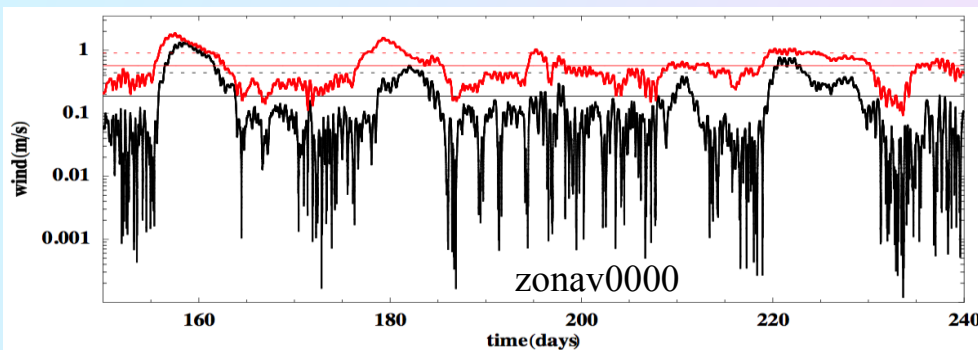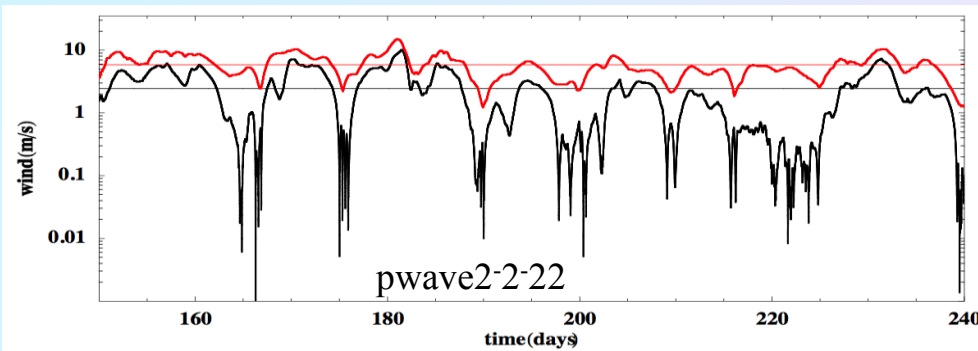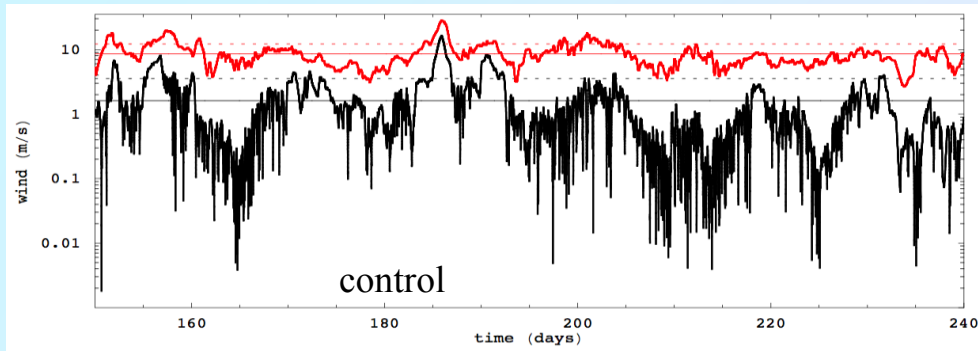
	control	pwave 2-2-22	zonave 0000
MX	28.2	14.9	1.86
AVE	8.58	5.84	0.57
MN	2.66	1.22	0.09
SD	3.63	2.39	0.34
SK	1.7	0.63	1.3

	control	pwave 2-2-22	zonave 0000
MX	16.4	10.0	1.32
AVE	1.61	2.45	0.19
MN	0.2e-2	0.7e-3	0.1e-3
SD	1.95	2.03	0.25
SK	3.1	0.86	2.4

Variances: meridional wind   Computation, cont.

control

altitude (km)

latitude (deg)

zonav0000

latitude (deg)

pwave2-2-22

altitude (km)

latitude (deg)
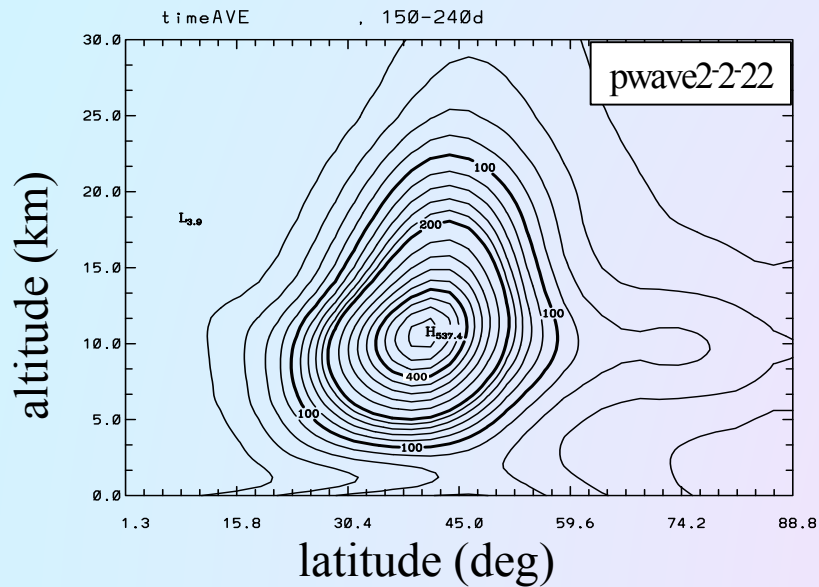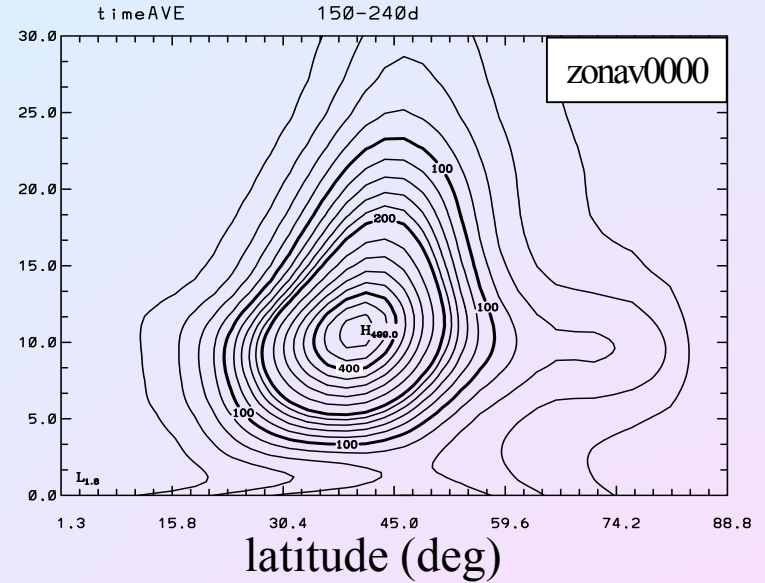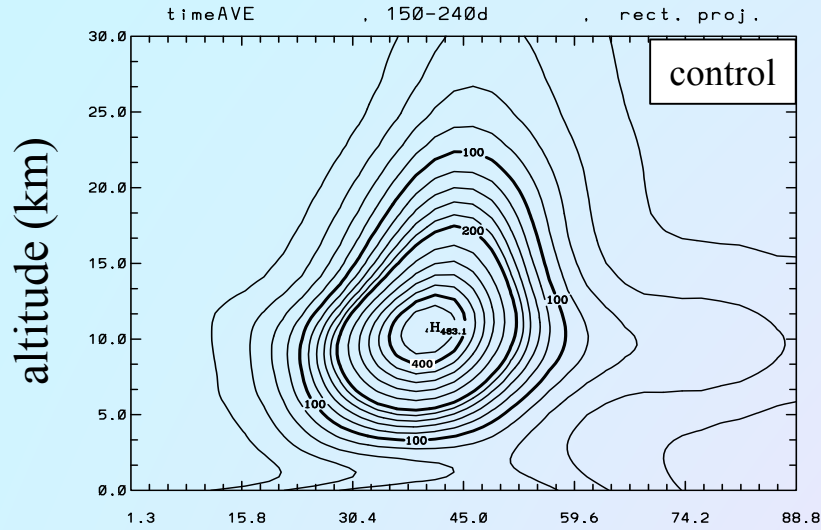
cnt = 20 m^{2}s^{-2} = cmin

RUN	MAX<(v')^2>
control	483
pwave2-2-22[&]	537
zonav0000[&]	499

[&]absorber: 2.78^0 x 30 min

Variances: zonal wind   Computation, cont.
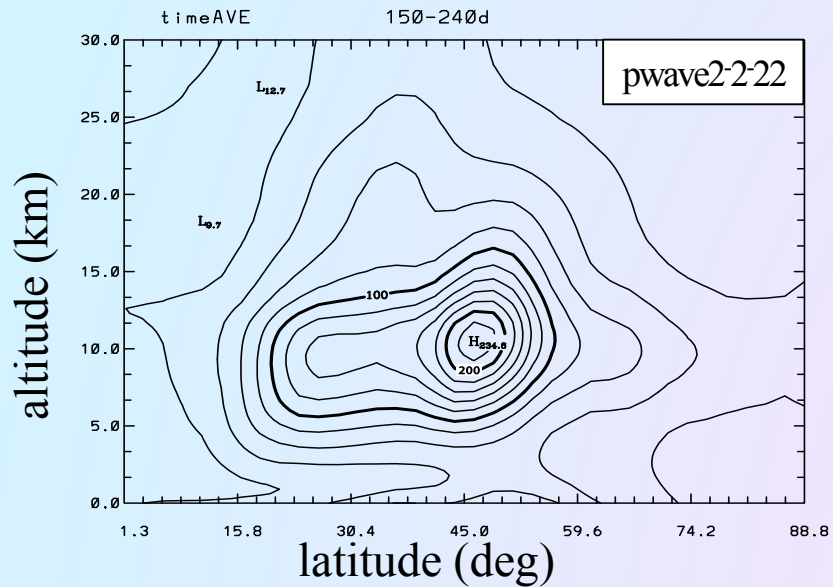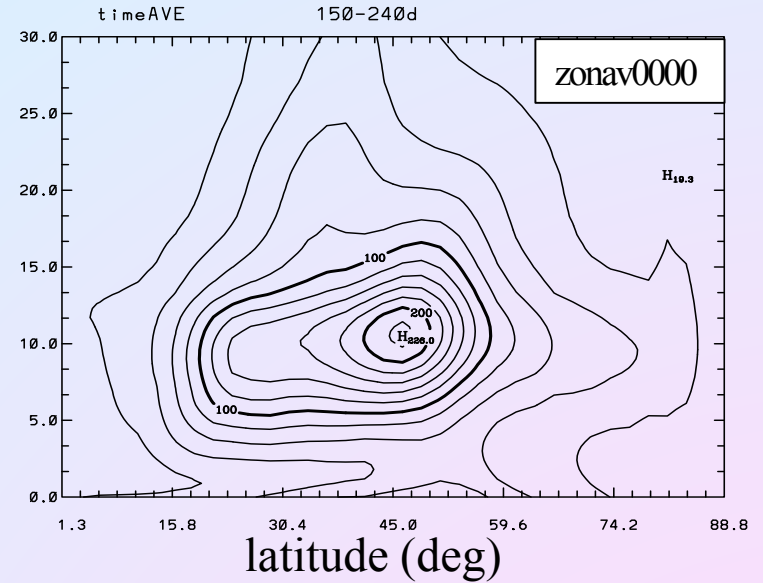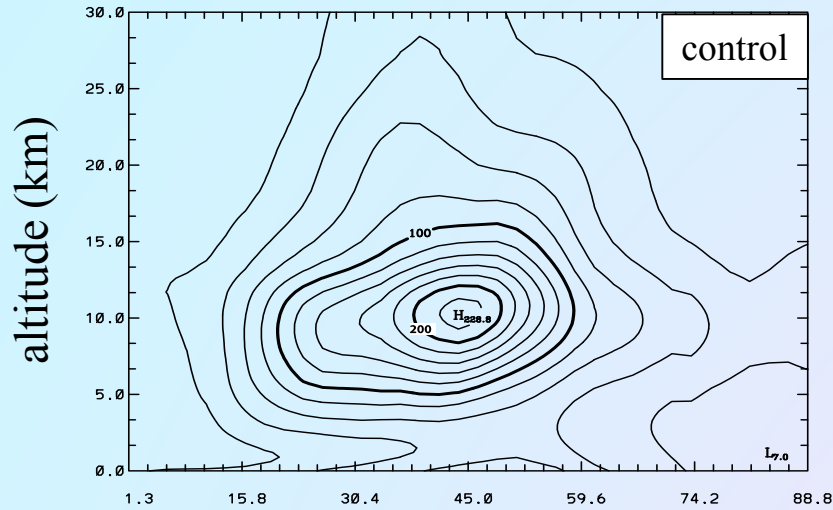
cnt = 20 m^{2}s^{-2} = cmin

RUN	MAX$<(v')^2>$
control	229
pwave2-2-22[&]	235
zonav0000[&]	226

[&]absorber: 2.78^0 x 30 min

Variances: vertical wind   Computation, cont.
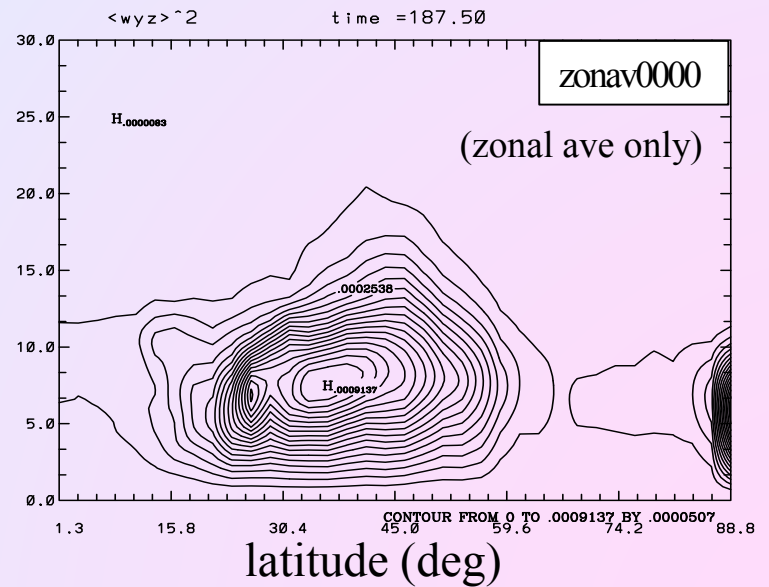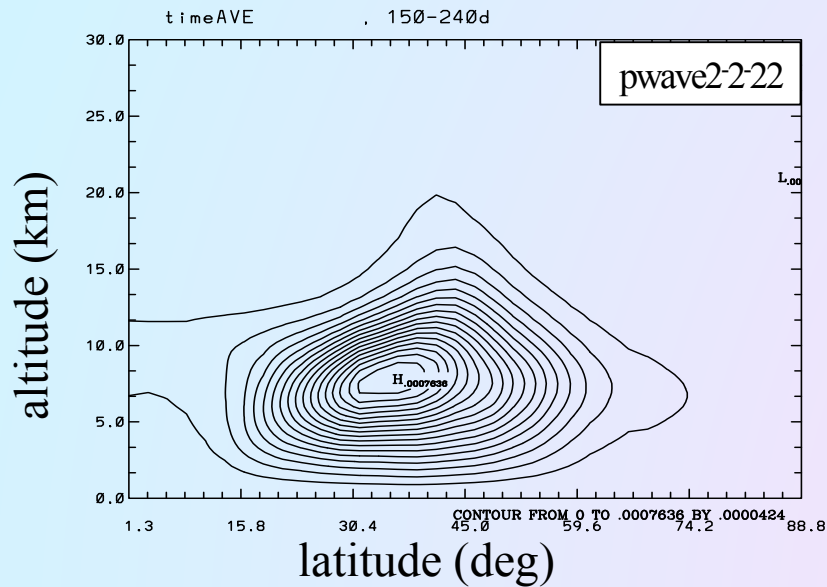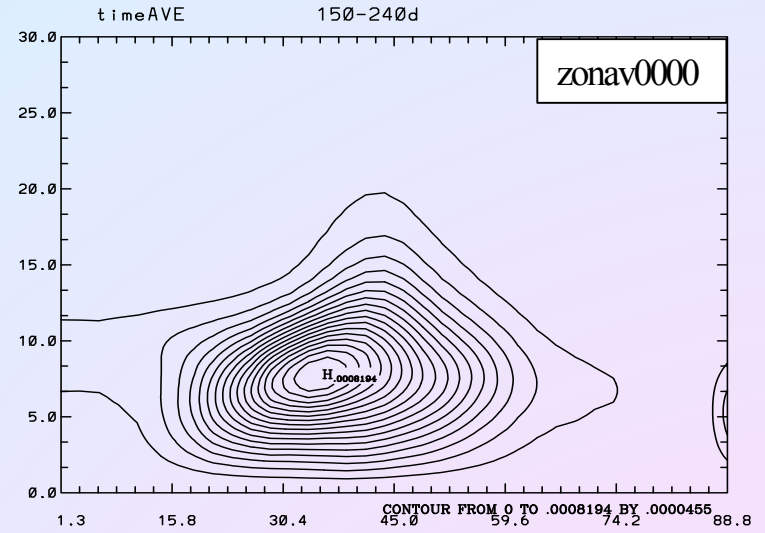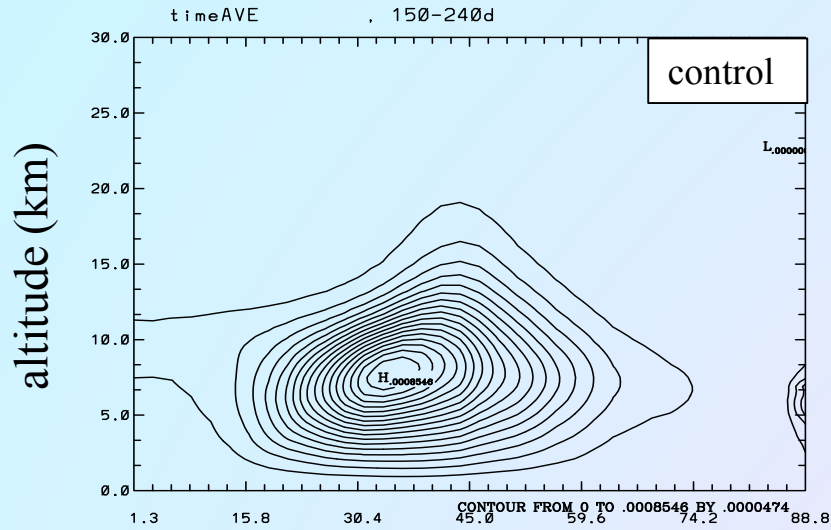
Averages of zonal wind
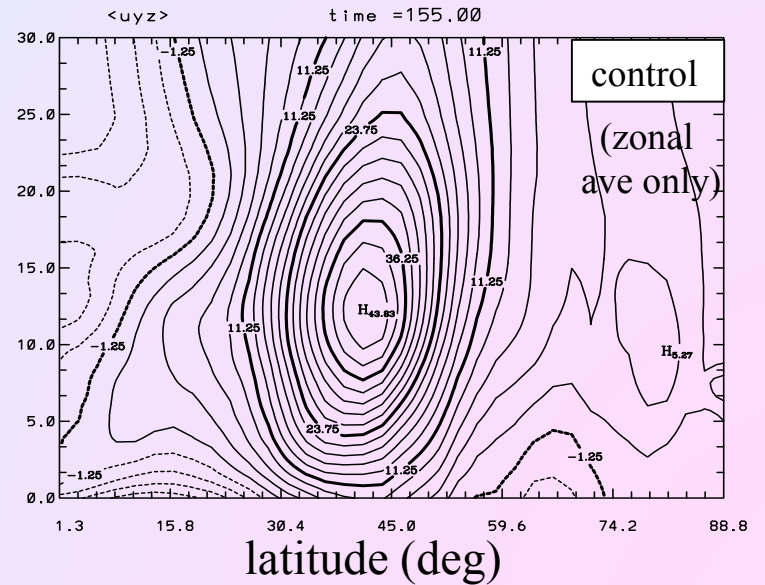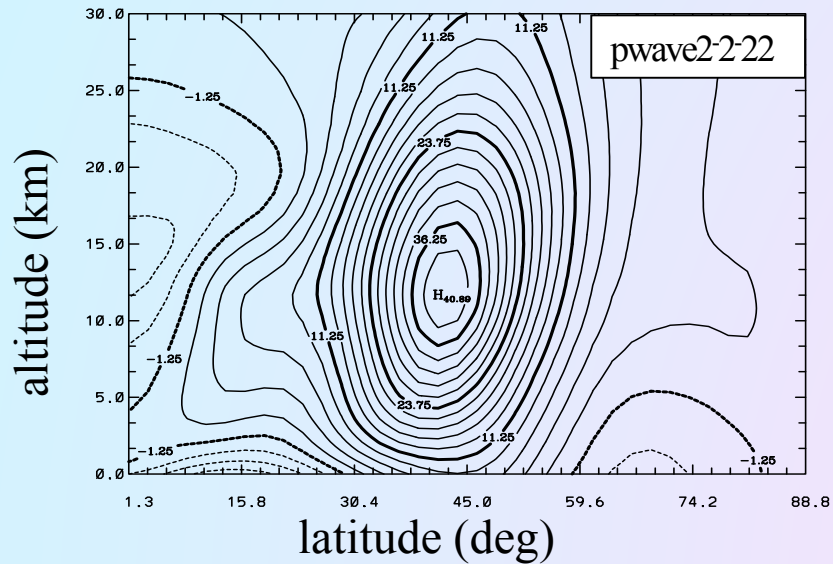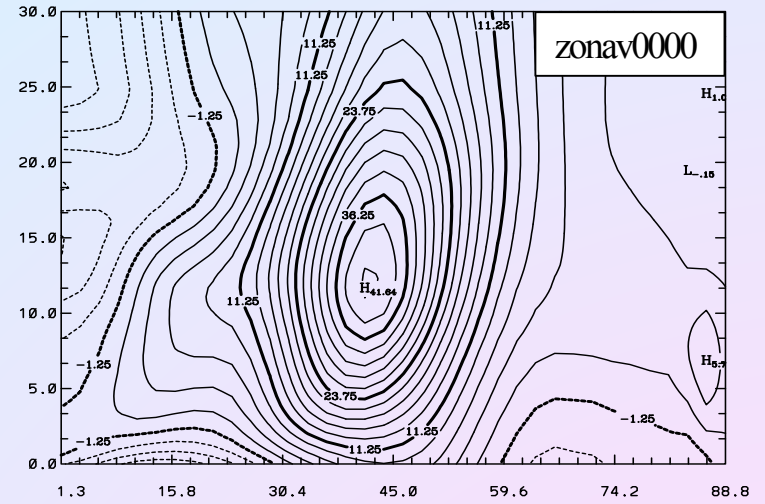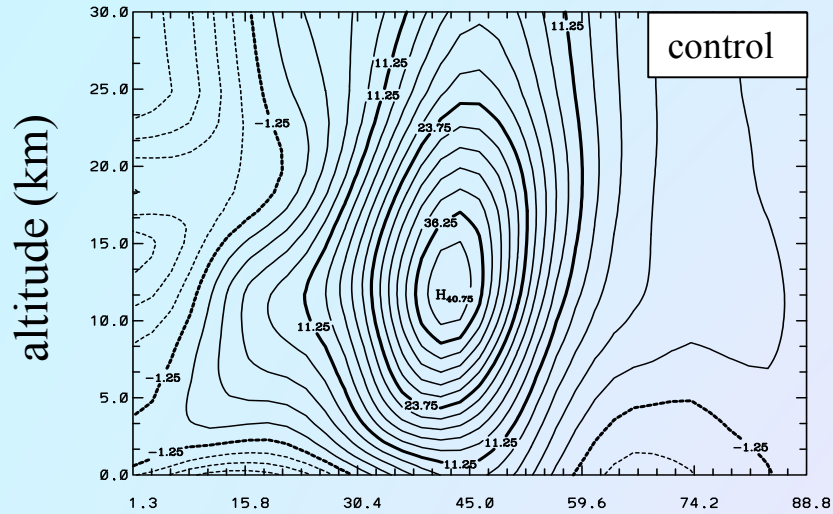
Summary for Polar Singularity Approach

• A multiscale asymptotic solution for flow at the pole is developed.

1. The *inner solution* valid at the pole: The horizontal wind components are:
$$u^+ = A \cos\lambda + B \sin\lambda \quad \text{and} \quad v^+ = B \cos\lambda - A \sin\lambda$$
Fundamental constraints on all vector differential operators.
Provides exact inner boundary condition for *middle solution*.

2. The *middle solution* in the polar neighborhood $0 \leq r \leq \varepsilon$ (where $r = \pm(\pi/2 - \phi)$ is the distance from the pole): Can be represented by Fourier series in azimuthal angle about the singularity.

3. The full computational result (*outer solution*): Used to evaluate the Fourier series coefficients.

4. The resulting middle solution is used in the implicit absorber of pressure solver.

•Computational results

1. Control simulation (no polar absorber) :
(a) Appears close to *inner solution* properties.
(b) Shows some minor pathologies which are extreme in zonav0000 simulation.

2. pwave2⁻2⁻22 simulation (new asymptotic absorber) :
(a) Overall solution very similar to control simulation.
(b) Much less noise near poles compared to control.
(c) Notably more stable than control.

3. zonav0000 simulation (pathological zonal averages only absorber) :
(a) Solution quite pathological near poles, flow activity anomalously low. Does not satisfy *inner solution* qualitatively.
(b) Computation allows much bigger timestep.

4. Other pwave simulations (not shown) :
(a) XXXX solution similar to X⁻X⁻XX but somewhat noisier and less stable for X=1,2,3.
(b) 3⁻3⁻33 similar to 2⁻2⁻22 but slightly less noisy and more stable.
(c) 2⁻2⁻22 notably better than 1⁻1⁻11 or 1⁻1⁻00 — gives a marked reduction in vertical wind field polar noise and improvement in stability.

5. Results 1-3 & 4a for case X=2 verified at higher resolution with (256 x 144) grid.

Comments/Future Directions

1. Optimum configuration of asymptotic solution for polar absorber not yet in hand

   → optimum absorber thickness and timescale?

   → increase number of modes according to grid point distance from pole?

2. Major increases in allowable Δt beyond ~ 2x that of the control unlikely due to explicit advection component.
   → fully implicit dynamical model for polar neighborhood?

3. Unstructured grid singularities?

1. Theoretical Preliminaries

Approximate continuous fields computed in the spherical shell by simplifying the local geometry of the polar neighborhood
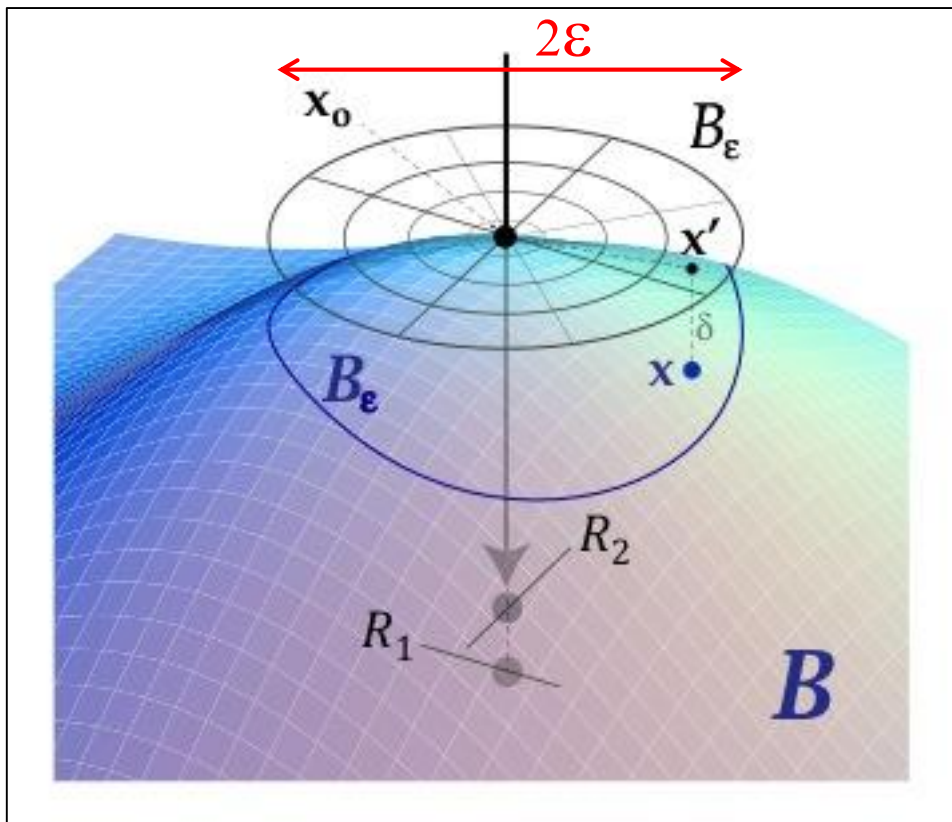
First geometrical
    approximation :

Restrict polar neighborhood to radius ε ST curvature is negligible:

define $K = \max(\,|\,\kappa_1(\mathbf{x})\,|,\,|\,\kappa_2(\mathbf{x})\,|\,)$ over all x in $\boldsymbol{B}_\varepsilon$, where κ_i is the curvature associated with R_i,

Then $\varepsilon K << 1$ ➔ $\delta/\varepsilon << 1/2$

Geodesic grids, cont.

642 vertices

Properties of the geodesic grids at different resolution

R	Number of cells N_c	Number of cells along equator	Average cell area in km^2	Ratio of smallest cell to largest cell	Average distance between cell centers in km	Ratio of smallest to largest distance btn cell centers
0	42	10	1.21e7	0.885	3717.4	0.881
1	162	20	3.14e6	0.916	1909.5	0.820
2	642	40	7.94e5	0.942	961.6	0.799
3	2562	80	1.99e5	0.948	481.6	0.790
4	10242	160	4.98e4	0.951	240.9	0.789
5	40962	320	1.24e4	0.952	120.5	0.788

$$N_c = 5 \cdot 2^{2R+3} + 2 \; ; \;\; R \geq -1$$

http://kilodot.com/post/3690269953/creating-a-geodesic-grid

2. Possibilities for other grids?   Geodesic

The area associated with grid point P_0 is the set off all points closer to P_0 than any other grid point.
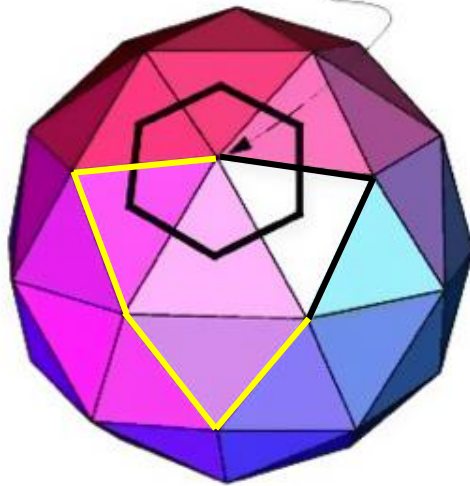
All of the resulting grid cells are hexagons, except for 12 pentagons.

The centers of the 12 pentagons are the 12 vertices of the initial icosahedron.

http://kilodot.com/post/3690269953/creating-a-geodesic-grid